NANO · MICRO small
www.small-journal.com

Nano-3D-Printed Photochromic Micro-Objects

Sebastian Ulrich, Xiaopu Wang, Markus Rottmar, René Michel Rossi, Bradley J. Nelson, Nico Bruns, Ralph Müller, Katharina Maniura-Weber, Xiao-Hua Qin, and Luciano Fernandes Boesel*

Molecular photoswitches that can reversibly change color upon irradiation are promising materials for applications in molecular actuation and photo-responsive materials. However, the fabrication of photochromic devices is limited to conventional approaches such as mold casting and spin-coating, which cannot fabricate complex structures. Reported here is the first photo-resist for direct laser writing of photochromic 3D micro-objects via two-photon polymerization. The integration of photochromism into thiol–ene photo-clickable resins enables rapid two-photon laser processing of highly complex microstructures and facile postmodification using a series of donor–acceptor Stenhouse adduct (DASA) photoswitches with different excitation wavelengths. The versatility of thiol–ene photo-click reactions allows fine-tuning of the network structure and physical properties as well as the type and concentration of DASA. When exposed to visible light, these microstructures exhibit excellent photoresponsiveness and undergo reversible color-changing via photoisomerization. It is demonstrated that the fluorescence variations of DASAs can be used as a reporter of photoswitching and thermal recovery, allowing the reading of DASA-containing sub-micrometric structures in 3D. This work delivers a new approach for custom microfabrication of 3D photochromic objects with molecularly engineered color and responsiveness.

1. Introduction

Stimuli-responsive materials based on molecular photoswitches can reversibly change color and other photophysical properties when a light stimulus is applied, enabling their remote control with high spatial and temporal precision.[1–3] The controlled change of properties upon light irradiation has been exploited for a broad range of applications ranging from photochromic ophthalmic lenses to optical switches, phase shifters, sensors, drug delivery, and actuators for soft robotics.[4–8] Most established systems, however, require UV light, which provides a very limited penetration depth into many materials or into skin, and is often detrimental to their structure.[9] These limitations have boosted the search for visible light-responsive photoswitches. One of the most remarkable developments in this field was the discovery of donor–acceptor Stenhouse adducts (DASAs), a new class of visible light-responsive photoswitches with negative photochromism.[10–12] With the rapidly increasing knowledge on their structure–property relationships and their subsequent optimization, 2nd and 3rd generation DASAs have overcome initial limitations, providing now access to the whole range of the visible spectrum with excellent photoswitching properties both in solution and in polymer matrices.[13–15] In materials science, DASAs have already been employed in multiple applications

Dr. S. Ulrich, Prof. R. M. Rossi, Dr. L. F. Boessl
Empa
Swiss Federal Laboratories for Materials Science and Technology
Laboratory for Biomimetic Membranes and Textiles
Lerchenfeldstrasse 5, St. Gallen 9014, Switzerland

Dr. S. Ulrich, Prof. N. Bruns
Adolphe Merkle Institute
University of Fribourg
Chemin des Verdiers 4, Fribourg 1700, Switzerland

Dr. X. Wang, Prof. B. J. Nelson
Institute of Robotics and Intelligent Systems
ETH Zurich
Tannenstrasse 3, Zurich 8092, Switzerland

The ORCID identification number(s) for the author(s) of this article can be found under https://doi.org/10.1002/smll.202101337.

DOI: 10.1002/smll.202101337

Dr. X. Wang
Shenzhen Institute of Artificial Intelligence and Robotics for Society
The Chinese University of Hong Kong
Shenzhen, Guangdong 518172, China

Dr. M. Rottmar, Prof. K. Maniura-Weber, Dr. X.-H. Qin
Empa
Swiss Federal Laboratories for Materials Science and Technology
Laboratory for Biointerfaces
Lerchenfeldstrasse 5, St. Gallen 9014, Switzerland

Prof. N. Bruns
Department of Pure and Applied Chemistry
University of Strathclyde
Thomas Graham Building, Cathedral Street 295, Glasgow G1 1XL, UK

Prof. R. Müller, Dr. X.-H. Qin
Institute for Biomechanics
ETH Zurich
Leopold-Ruzicka-Weg 4, Zurich 8093, Switzerland
E-mail: qinx@ethz.ch

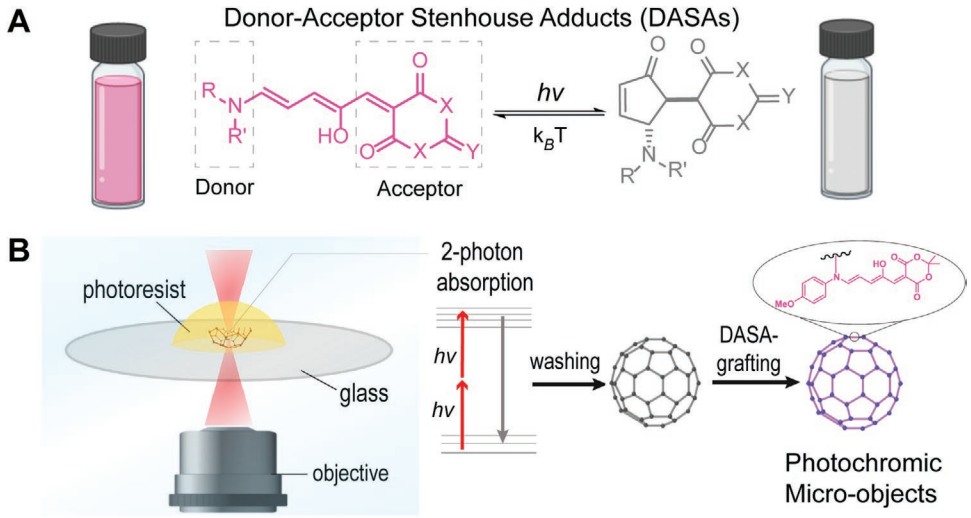

Figure 1. Strategy for 3D-printed photochromic micro-objects. A) General structures for donor–acceptor Stenhouse adducts (DASAs) and their photoswitching between the open triene (colored) and the closed cyclopentenone (colorless) isomers. R/R′: alkyl or aryl; X: O or N. B) Schematic of ultrafast direct laser writing of complex polymeric microstructures by two-photon polymerization (2PP) and subsequent functionalization with DASA photoswitches.

from sensors to wavelength-specific photopatterning and visible light responsive enzyme nanoreactors.[16–26] In such multi-addressable materials, DASAs serve as molecular logic gates that only require different visible light sources to control the different states.[27,28] To date, however, DASAs have been studied mostly in 2D substrates such as polymer films and modified surfaces, which impedes the study of photochromism in defined 3D structures. Combining the wavelength-specific activation of DASAs with complex-shaped objects could allow the fabrication of materials with sophisticated control both on the functional and the structural level. Approaches to fabricate customized 3D photochromic objects have yet to be established.

Recent advances in 3D-printing technologies have witnessed their burgeoning applications in soft robotics, microelectronics, and biomedicine.[29–31] One of the most precise 3D-printing technologies is two-photon photolithography (2PP),[32,33] which relies on localized curing of liquid ink materials upon nonlinear two-photon photoinitiation triggered by an ultrafast near-infrared laser beam. Since most polymeric materials are transparent at 800 nm, one can easily build custom 3D micro-objects in accordance with computer-aided design,[32] or even control material properties in space and time at sub-micrometer-level resolution.[33,34] Radical-mediated thiol–ene click reactions are particularly suitable for photocrosslinking due to their high reactivity and selectivity through the fast initiation with radical photoinitiators and subsequent chain-transfer reactions.[35,36] While a number of photoresists have been developed for 2PP in recent years,[37] so far there are no materials and methods for digital 3D fabrication of complex micro-objects that allow dynamic tuning of color on demand.

Herein, we describe a new approach to fabricating visible light-responsive photochromic 3D micro-objects by interfacing a modular thiol–ene resin with nanoscale 3D-printing technique based on 2PP (**Figure 1**). We firstly designed and formulated a highly efficient thiol–ene photo-clickable resin that consists of multifunctional thiols/enes and an ene-terminated DASA precursor. This material is robust for thiol–ene photocrosslinking and enables ultrafast laser microfabrication of complex 3D objects at high writing speeds up to 50 mm s^{-1}. The microstructures can be functionalized with a series of DASA photoswitches with wavelength-specific switching properties in a modular manner. By scanning a focused green laser inside the functionalized microstructure, dynamic color-tuning of DASA-containing polymer networks at high spatial resolution as well as their reversible photoswitching could be realized.

2. Results and Discussion

As depicted in **Figure 2**, the resin is composed of off-stoichiometric mixtures of pentaerythritol tetra(3-mercaptopropionate) (PETMP, 4Thiol), triallyl-1,3,5-triazine-2,4,6-trione (TATATO, 3Ene), and an ene-terminated DASA precursor (4-methoxy-*N*-(pent-4-en-1-yl)aniline, EnePre) from a two-step synthesis. Using diphenyl(2,4,6-trimethylbenzoyl)phosphine oxide (TPO) as the photoinitiator, an off-stoichiometric thiol–ene photocrosslinking was performed upon exposure to either UV light for one-photon curing (315 nm) or near-infrared laser pulses for 2PP (780 nm).

After developing these networks in a solution of activated furan adducts (FAs) where the DASAs are formed by reacting with the aromatic amine of the DASA precursor, photochromic DASA polymer networks were generated. Figure 2C shows three different FAs based on Meldrum's acid (Meld), N-substituted barbituric acid (Barb) or a pyrazolone (Pyra). While the first two FAs have been employed already in the first reports of DASA photoswitches,[14] Pyra was the first of a new set of FAs, pushing the DASA absorbance toward higher wavelengths (675 nm).[20] The precursor-based approach offers several advantages: first, it minimizes the risk of photodamage to DASAs during photopolymerization as a result of laser irradiation within the absorption range of DASAs, but keeps the capacity to fabricate 3D micro-objects composed of DASA-networks through nanoscale 3D-printing via 2PP. Second, simple variation of the FAs provides access to multiple DASAs with different colors and photoswitching properties from the same

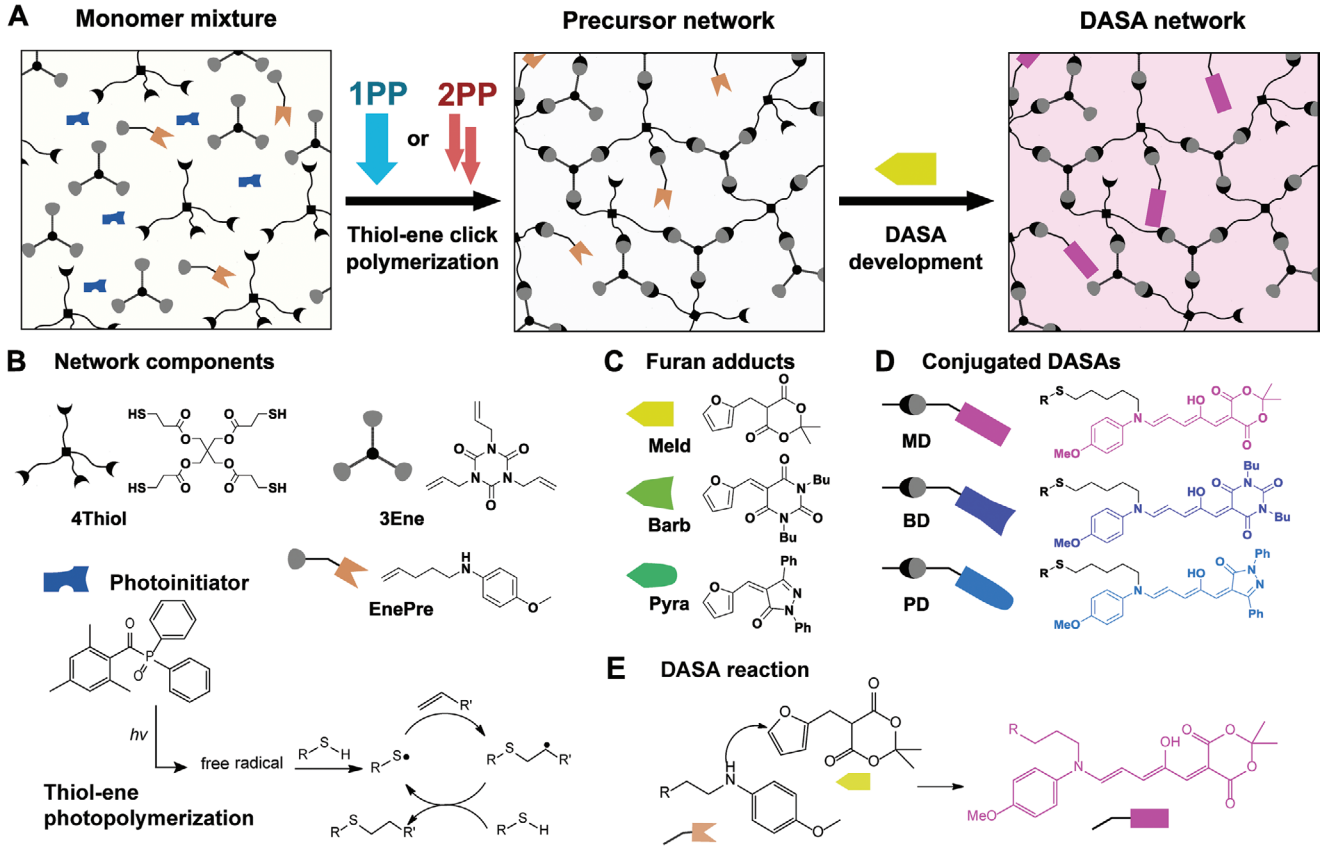

Figure 2. A) Design of a modular thiol–ene resin for custom fabrication of DASA-networks by one-photon polymerization (1PP) or two-photon polymerization (2PP) and subsequent DASA development. B) Chemical structures of network components (4Thiol, 3Ene, EnePre) and the mechanism of photoinitiated thiol–ene photopolymerization. C,D) Chemical structures of three activated furan adducts (FAs: Meld, Barb, or Pyra) (C) and the formed DASAs (D) based on Meld (MD), Barb (BD), and Pyra (PD), respectively. E) Schematic of the DASA reaction between the EnePre and Meld.

precursor network. With the rapid development of new FAs, the approach can be expanded to include novel DASA types with different or improved properties and functionalities. Finally, by varying the stoichiometry of thiol–ene monomers, the network structure, composition, and mechanical properties can be tuned to optimize their performance as a photochromic matrix.

To investigate the thiol–ene click photopolymerization and the resulting network properties, we synthesized a number of networks with different compositions by tuning the stoichiometry of the monomers (see **Table 1** for samples and their nomenclature). After development of a network of, e.g., 2:1-1 with Meld toward the Meldrum's acid-based DASAs, it was termed 2:1-1MD (please see Table 1 for an explanation of the nomenclature). Accordingly, it was termed 2:1-1BD for Barb and 2:1-1PD for Pyra, with MD, BD, and PD designating the Meld-, Barb-, and Pyra-based DASAs (Figure 2D). Due to the intense color of DASAs, with molar extinction coefficients of the open form in the range of $\approx 10^5$ M^{-1} cm^{-1},[10] only small amounts of DASAs are typically needed to provide strong coloration.

The chemical compositions of our resins were investigated by attenuated total reflectance Fourier-transformed infrared (ATR-FTIR) spectroscopy. **Figure 3**A depicts the FTIR spectra of different precursor networks and for comparison the spectra of the monomers and EnePre are shown in Figure S2 of the Supporting Information. The different compositions of the networks are mirrored by the relative intensities of the

Table 1. Properties of precursor and DASA-networks (see Table S1 of the Supporting Information for additional networks).

Network[a)]	Thiol: Ene[b)]	$Ene_{Monomer}$: EnePre[b)]	T_g[c)] [°C]	S_{Vol} (acetone)	G'/G''[d)] [MPa]	tan δ[d)]	G[a),d)] [MPa]	$t_{3/4}$[e)] [min]
2:1-1	2:1	100:1	−8/−7/−5	1.5 ± 0.03	1.5 ± 0.2/0.15 ± 0.01	0.10 ± 0.01	1.5 ± 0.2	74
1:1-1	1:1	100:1	17/7/11	1.2 ± 0.02	2.9 ± 0.9/1.8 ± 0.4	0.61 ± 0.13	3.4 ± 0.1	159
1:2-1	1:2	100:1	10/8/10	1.4 ± 0.02	2.9 ± 0.2/1.5 ± 0.01	0.51 ± 0.03	3.2 ± 0.2	111

[a)]Example of nomenclature: 2:1-1 = network formed by a monomer mixture with a thiol:ene ratio of 2:1, and 0.01 molar equivalent of EnePre to the ene functional groups of the monomer; [b)]Ratio in monomer mixture; [c)]Determined by DSC before/after washing of network/after DASA development with Meld; [d)]Determined by in situ photorheology and dynamic rheology.[e)]Time required to reach 75% of the final absorbance value during the recovery experiments (Figure 4D).

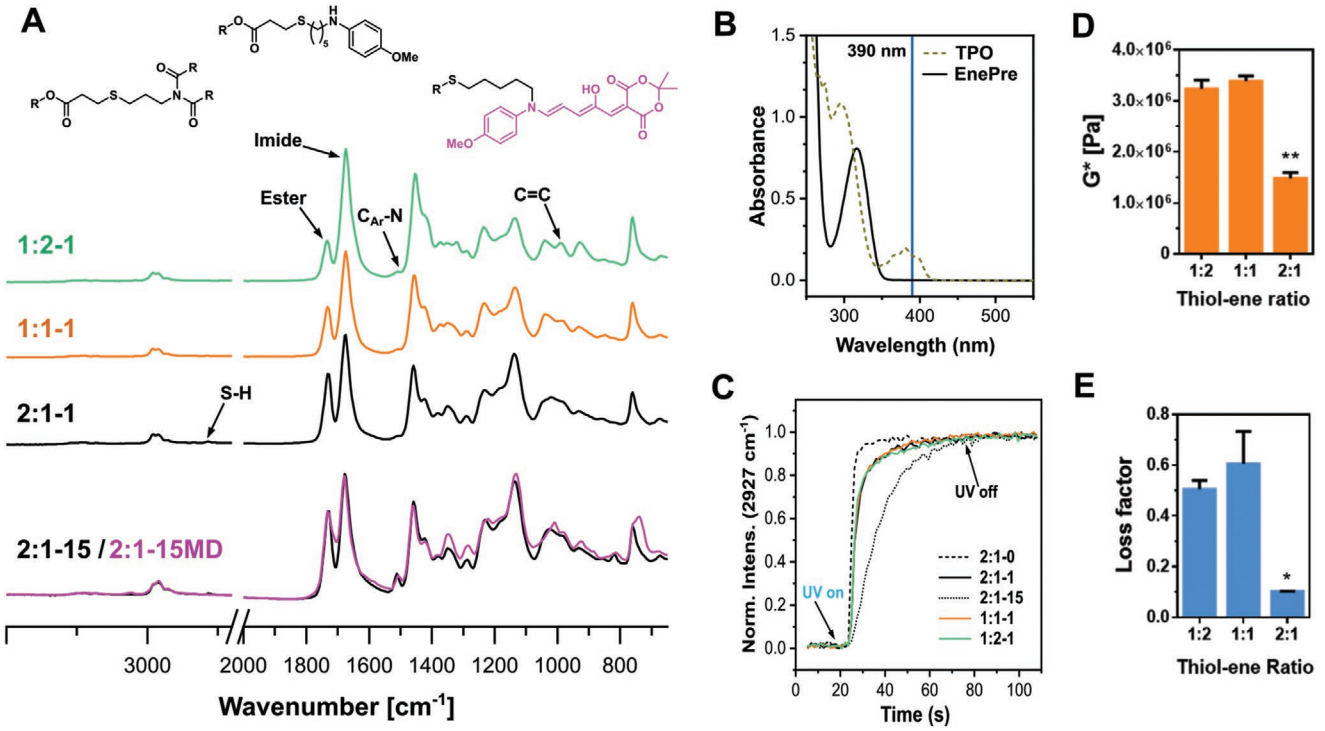

Figure 3. A) ATR-FTIR spectra of precursor networks with different network compositions and one DASA-network. The spectra show key features of the network molecular structures, derived from the precursor monomers (see Figure S2, Supporting Information). B) UV–vis spectra of the TPO initiator and EnePre: single-photon absorption at 390 nm, corresponding to half of the laser center wavelength (780 nm) for two-photon photolithography is marked with a blue line. C) In situ monitoring of thiol–ene photopolymerization kinetics of networks with different compositions using ATR-FTIR (see Figure S6C of the Supporting Information for statistics). D,E) The effect of thiol–ene ratio on matrix mechanics – complex modulus (G^*) and loss factor as determined by photorheology. Data are shown as mean ± sd (* $p < 0.05$, ** $p < 0.01$).

ester peak of 4Thiol (1730 cm^{-1}) and the imide peak of 3Ene (1674 cm^{-1}). An excess of ene groups in the monomer mixture (1:2-1) resulted in the complete disappearance of the thiol signal at 2562 cm^{-1} while an excess of thiol groups (2:1-1) resulted in the disappearance of the ene signal at 924 cm^{-1}. The disappearance of both signals for an equal ratio (1:1-1) indicates a high conversion of the functional groups during thiol–ene photopolymerization. A high degree of monomer incorporation into the network is supported by the small difference between unwashed precursor networks and ones that were washed in organic solvent (Figure S4, Supporting Information). Comparison of full spectra from the early and late stages of the polymerization further confirmed that functional groups are consumed during the 1PP process and not removed later during the washing step (Figure S6A, Supporting Information). The successful incorporation of EnePre was confirmed by the appearance of a characteristic peak of the aromatic amine at 1512 cm^{-1}. Higher concentrations, for example for 2:1-15 and for 2:1-3 were incorporated into the networks as well, demonstrating good control over the degree of network functionalization (Figure 3A – bottom; Figure S5, Supporting Information).

Next, we investigated the kinetics of thiol–ene photopolymerization (1PP) by in situ ATR-FTIR. The peak at 2927 cm^{-1} corresponds to the formation of a methylene group during the polymerization. The monomer mixture without EnePre reacted extremely fast, being cured after an exposure to UV light for 3 s (t_{90} = time required to reach 90% of the maximum normalized intensity in the FTIR curve), indicating the excellent efficiency of radical-mediated thiol–ene click reaction (Figure 3C). Monitoring at different wavelengths corresponding to the C_{vinyl}—H bond (3075 cm^{-1}), the thiol group (2562 cm^{-1}), or the vinyl group (924 cm^{-1}) gave the same result (Figure S6B, Supporting Information). Furthermore, independent repetitions of the experiments confirmed excellent reproducibility (Figure S6C, Supporting Information). Notably, the stoichiometry of the main monomers (4Thiol and 3Ene) did not have any observable effect on the polymerization kinetics until late stages of reaction: a significant effect of the composition could only be observed at 90% conversion or higher (Figure S6C, Supporting Information). At this point, however, gelation already occurred, and the differences in conversion at any time point never exceeded 2%, so that the effect of composition can be neglected. The presence of EnePre retarded the polymerization in a concentration dependent manner, though it still occurred within 20 s (t_{90}) for the practically relevant formulations with 0.01 eq. of EnePre (and t_{90} = 31 s for formulations with 0.15 eq of EnePre). The retarding effect of EnePre can be explained by the overlap of its absorption spectrum with the one of TPO initiator in the UV region (Figure 3B). However, such an overlap does not exist during the two-photon absorption of TPO at 780 nm. Therefore, 2PP can be expected to occur without interference.

The physical properties of a polymer matrix, in particular its stiffness/softness and the amount of polymer free volume can

impede or allow the required dynamic motion on the molecular level during photoswitching.[38,39] Therefore, we utilized in situ photorheology (Figure S7, Supporting Information) to assess the mechanical properties and photoreactivity of the resulting networks. Soft polymer matrices from low-T_g polymers generally provide the best conditions for the photoswitching of photochromic compounds with large changes in molecular shape.[40] Previous reports on DASAs that isomerize from a linear extended form into a cyclic and compact form have emphasized the importance of such matrix properties, with only soft low-*Tg* matrices enabling good performances.[14,23]

The measurements confirmed the fast polymerization kinetics. All changes occurred within 3 s, which is the time resolution of the photorheology setup. The speed of the network formation as determined by photorheology appears to be even faster than in the FTIR experiments. The difference is explained by the use of multifunctional monomers in a step-growth polymerization that results in an early gel point, i.e., network formation when a portion of the functional groups is still reacting, a behavior already observed by us for other multifunctional polymerizations. The mechanical properties of the networks were found to strongly depend on the ratio of the monomer components (Figure 3D): A much softer network was obtained from the thiol-rich 2:1-1 composition in comparison to the networks from the ene-rich 1:2-1 or thiol–ene equimolar 1:1-1 compositions. Both the molecular structure of the monomers and the crosslinking density of the networks determine their mechanical properties. The more rigid structure of 1:1-1 indicates that the crosslinking density plays a major role. Moreover, the more rigid molecular structure of the cyclic 3Ene monomer appears to result in a more rigid network (1:2-1 vs 2:1-1). With the contributions of both lower crosslinking density and lower amount of rigid monomers, the loss factor of 2:1-1 networks (Figure 3E) is about 0.1, which is much lower when compared to the other two networks. The lower the loss factor, the weaker the damping properties of the networks.

Furthermore, we employed dynamic rheology to assess the deformability of the networks. Dynamic frequency sweep experiments (Figure S7C, Supporting Information) show a clear difference in network structure. For the stiffer networks, the storage modulus (G') and loss modulus (G'') are cross-sectioned at high angular frequencies. By contrast, the G' of soft networks (2:1-1) remain constantly higher than G'' in the whole range, indicating a distinct difference in microstructure compared to the other two networks.

The difference in mechanical properties suggests a difference also in the thermal properties of the networks. To verify this hypothesis, the networks were analyzed by differential scanning calorimetry (DSC). For the softest network 2:1-1, a glass transition temperature (T_g) of −8 °C was found, whereas the T_g of the stiffer networks was closer to room temperature (Figure S8, Supporting Information). Interestingly, washing of the 1:1-1 networks resulted in a decrease in T_g by several degrees (Table 1). With the loss of a large amount of residual monomer and oligomers being highly unlikely, we suggest a decreased ability to cope with the mechanical strain during swelling of this more rigid network with a higher degree of crosslinking density due to the stochiometric ratio of vinyl and thiol functionalities. Accordingly, no such difference was observed for networks 2:1-1 or 1:2-1.

The optically transparent precursor networks turned into colored DASA-networks (**Figure 4**A) after the reaction with FAs. Monitoring this reaction with 2:1-15 using FTIR revealed that the reaction takes up to several days and no further reaction occurred after ≈7 d (Figure S9, Supporting Information). Due to the relatively slow reaction, which is typical for 2nd generation DASAs based on aromatic amines with low nucleophilicity,[20,23] the degree of DASA functionalization can be adjusted not only by the amount of EnePre in the precursor network but also by the duration of the DASA development step. In fact, we limited the reaction time for several samples since fully reacted DASA-networks from a 100:1 ene–EnePre ratio were often too intense in color to be analyzed by UV–vis spectrometry.

Variation of the FA type enabled the generation of three different DASA-networks with peak absorbance values of 562 nm (MD), 590 nm (BD), and 616 nm (PD), covering an overall absorbance range of more than 200 nm (Figure 4B). Importantly, photoswitching occurred for all network compositions and for all DASA types with the complete loss of color under white light irradiation and thermal reversion to the colored state in the dark (Figures S9 and S10, Supporting Information). Figure 4C shows the loss of the characteristic absorption peak of DASA in the 2:1-1MD network upon white light irradiation.

In our previous work, we found a strong dependency of both the DASA photoswitching and the thermal back-isomerization on the T_g of the matrix polymer, with a rigid matrix impeding or even preventing it entirely.[23] As described above, all networks possessed glass transitions below room temperature, and the T_g for the 2:1-1 network was increased from −8 to −5 °C after the FA reaction (Table 1; Figure S7, Supporting Information). To investigate the influence of matrix mechanics on the DASA behavior, we monitored the thermal recovery in the dark for the different network compositions. Interestingly, the recovery rate was found to strongly depend on the specific network type (Figure 4D and Table 1): the $t_{3/4}$ (the recovery time of 75% of the initial absorbance) increased from the soft matrix to 1:1-1MD as the most rigid and crosslinked network, suggesting that the soft network favors a fast response. In addition to the network composition, the structure of DASAs also influenced the recovery rate: the Pyra-based PD recovers faster in comparison to BD and to MD (Figure S11D, Supporting Information). These results are in line with our previous findings[20,23] and underline the importance of tuning the matrix properties as well as carefully choosing the DASA type to achieve the desired photoswitching performance.

DASAs are generally susceptible to degradation by strong nucleophiles and, accordingly, free thiols in the networks can result in the degradation of part of the DASA population during the development step or even over time.[12] Indeed, we found a decrease in color intensity from the 1:2-1MD network over 1:1-1MD to network 2:1-1MD (Figure S10, Supporting Information). The 1:2-1 MD network has the highest color intensity presumably due to the absence of thiols that cause partial DASA degradation. Accordingly, we could in the future produce soft networks without residual thiols from a sub-stoichiometric amount of thiol. One possibility would be co-macromonomers,

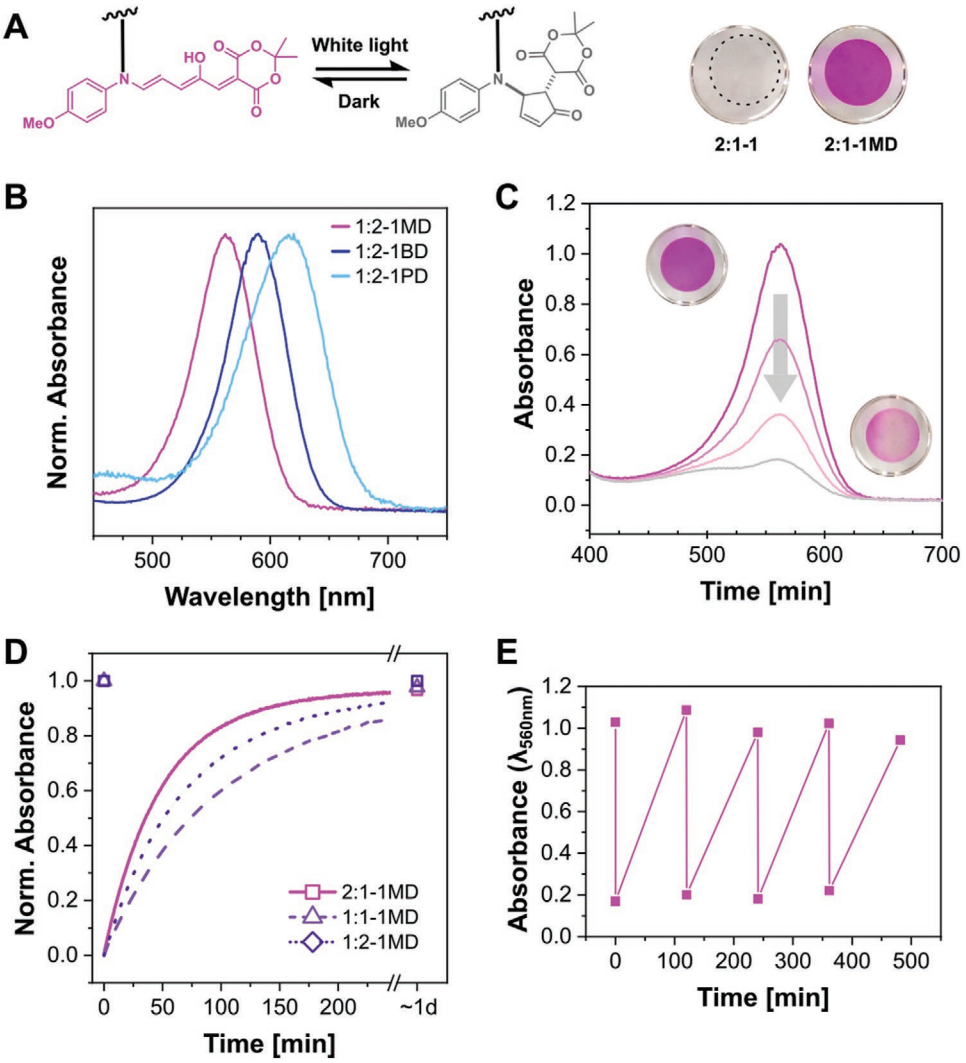

Figure 4. A) Schematic depiction of the photoisomerization of a DASA-containing network (MD) with open (colorful) and closed (colorless) state. The photos on the right show images of network before and after development (2:1-1 and 2:1-1MD). B) UV–vis spectra of three different DASA-networks derived from one precursor network. The networks are partially photoswitched to reduce the peak intensity to the range of the spectrometer. C) Spectra of 2:1-1MD before and after incremental photoswitching by white light irradiation (each spectrum corresponds to additional 10 s of irradiation). D) Back-isomerization in the dark (at room temperature) of photoswitched DASA-networks of different composition. Due to the high absorbance values, the recovery could not be monitored from the peak wavelength for all networks (560 nm for 2:1-1MD, 586 nm for 1:1-1MD and 520 nm for 1:2-1MD). Point of irradiation: $t = 0$. E) Cycling of 2:1-1MD between colorful and colorless state by repeated irradiation (30 s) and recovery in the dark (120 min).

for example ene-functional silicones. They would, in addition, increase the softness of the network due to a plasticizing effect.

With the superior photoswitching properties of the 2:1-1 network when compared to the other two (Table 1), we chose this resin for nanoscale 3D-printing of photochromic micro-objects via 2PP. To this end, a commercial Nanoscribe GT 3D microprinter was applied to screen the processing window of this resin and to fabricate photochromic objects with user-dictated complex structures (**Figure 5**A). As shown in Figure 5B, we first fabricated simplified line-like structures at varying scanning speeds (100 µm s^{-1}–10 mm s^{-1}) and laser power (10 to 50 mW). At 10 mm s^{-1} or even higher speeds, arbitrary microstructures can be printed by increasing the Line Number or increasing the laser power. The robust thiol–ene reactions enabled rapid controlled fabrication of reproducible microstructures at writing speeds up to 50 mm s^{-1} (Figure S14, Video S1, Supporting Information), which is the upper limit of the device.

We then investigated the dynamic patterning (spatial and temporally resolved) of 3D micro-objects fabricated via 2PP (Figure S13, Supporting Information). By irradiating the object with a focused green laser (561 nm) in a confocal microscope, arbitrary 3D micropatterns were generated at high spatial resolution and in a sequential manner (Figure S13A,B, Supporting Information). The reversibility of the patterning process was monitored via time-lapse imaging of the transmission light intensity within the region of interest (ROI) area (Figure S13C, Supporting Information). These results demonstrate that complex and reversible photopatterns can be written with visible light into DASA-based 3D micro-objects.

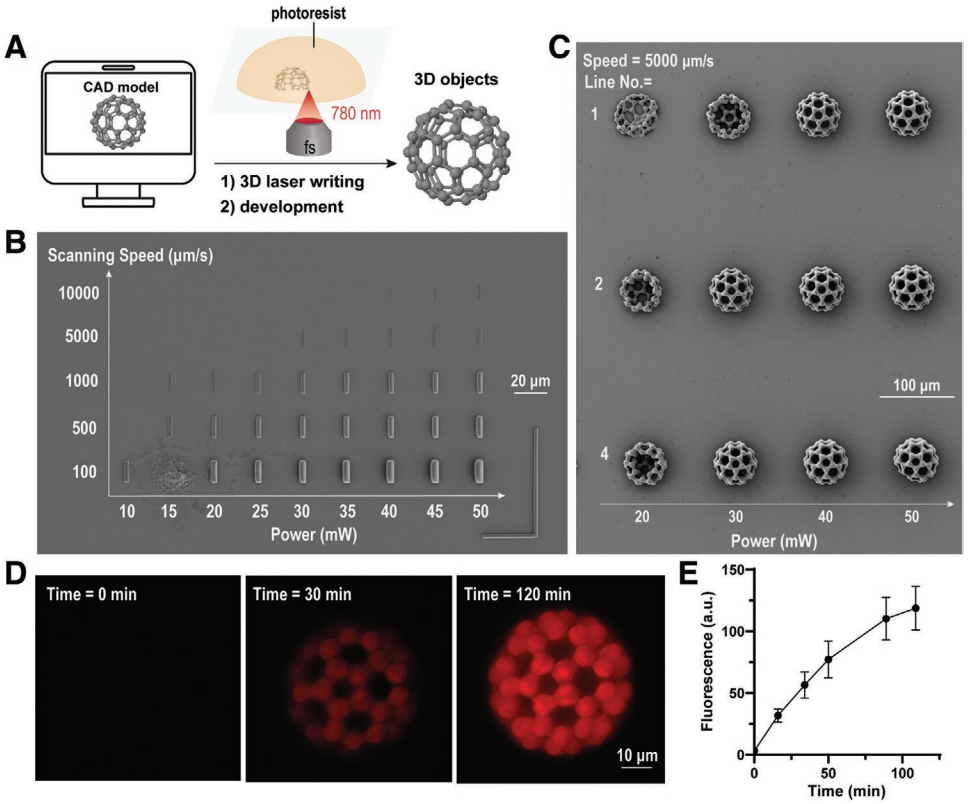

Figure 5. Nanoscribe 3D-printing via 2PP, functionalization, and photoswitching of color-changing fullerene-shaped microstructures prepared with a 2:1-1 network. A) Schematic of direct laser writing using a C_{60}-shaped CAD model. B,C) SEM images of microprinted rectangular structures at varying scanning speed and laser power (B) and complex C_{60} microstructures at varying line number and laser power (C), PowerScaling = 1. D,E) After development, functionalization, and laser excitation, the C_{60} microstructures are photoswitchable. D) Microscopic images of the microstructures at different time points after laser excitation. E) The thermal recovery kinetics of DASA-containing networks could be precisely monitored by the fluorescence.

Furthermore, we fabricated more complex 3D microobjects using a C_{60}-shaped CAD model. Since this model has a spherical shape, the initially printed microstructures tended to collapse or distort, presumably due to the limited interfacial bonding depth (<1 μm) despite the use of thiol-functionalized glass substrate. To address this, we optimized the printing process by increasing the bonding depth to 5 μm to enhance the stability of microprinted structures. Furthermore, we found that the increase of Line Number from 1 to 2 and to 4 could also greatly enhance the structural stability after development in acetone (Figure 5C). There was no measurable shrinkage based on the SEM data, which are in line with other studies on thiol–ene resins that typically show low shrinkage.[41] This is likely due to the fact that the employed laser power which was well above the polymerization threshold.[41] The resolution of a thiol–ene resin in 2PP can reach about 300 nm as reported elsewhere.[42]

Finally, we studied the feasibility of incorporating DASA into the 3D microprinted networks as well as the photoswitching properties thereof. The printed microstructures were reacted with one type of FA (Meld) for 12 h protected from light to incorporate the DASA into the network. The shortened duration for this reaction is based on the fact that the structures are porous with sizes of ≈50 μm, thereby facilitating the DASA reaction. Unlike the samples prepared by 1PP, the printed microstructures have a different brightness. This is likely due to the variations in photoinitiation kinetics and photon intensity between 1PP and 2PP.

Due to the small scale of these structures that renders UV–vis spectrometry unavailable for their investigation, we decided to employ the fluorescence of DASAs to monitor photoswitching and recovery of nano-3D-printed photochromic structures. Mason et al. have previously shown that the fluorescence of the open form of alkylamine-based DASAs can be used to track the closed-open transition, though this work did not include reversible photoswitching.[18] To our knowledge, no previous work has employed the change in DASA fluorescence to monitor their photoswitching transition in solution or covalently immobilized in a polymeric matrix. Yet, it presents a method toward quantitative information on the DASA state even in miniature complex structures. First, we investigated the fluorescence of the aromatic amine-based DASA in solution and in 2:1-1MD networks. We found that the DASA solutions and networks have weak fluorescence in the open state (Figure S12, Supporting Information), with maximal fluorescence of DASA in the open state at 615 nm. Once irradiated with white light, the fluorescent intensity of DASA disappeared due to the transition into the colorless and nonfluorescent closed state upon switching. Furthermore, the recovery of fluorescence in DASA networks reached >95% of the fluorescence before switching, and

100% in DASA solutions (Figure S12, Supporting Information), much in accordance with our previous UV–vis experiments.

We applied these findings to characterize the switching behavior of our structures. The 3D microprinted fullerene structures were, first, photobleached by green laser irradiation at 546 nm for 2 min on a Zeiss LSM880 laser microscope. Subsequently, time-lapse confocal imaging was performed to monitor the fluorescence recovery of DASA-containing networks inside the microstructure. As shown in Figure 5D, the fluorescence of DASA in the microstructure recovers after within 120 min. Moreover, the fluorescence intensity could be quantified and plotted as depicted in Figure 5E. This demonstrates that the fluorescence of DASA photoswitches can be utilized to study the reversible switching and recovery of these photochromes, allowing the reading of DASA-containing polymer matrices in 3D.

3. Conclusion

In conclusion, we developed a modular thiol–ene resin for custom microfabrication of visible light-responsive polymer networks with covalently attached DASA photoswitches. UV photocrosslinking allows facile preparation of thin films while direct laser writing by 2PP with near-infrared laser pulses enables ultrafast custom microfabrication of 3D objects with complex geometry. The photoswitching properties of the networks depend strongly on the stoichiometry of the monomers and the resulting mechanical properties of the polymer networks, with softer networks enabling faster DASA isomerization. The described ink system provides excellent control over the composition and the geometry of the networks, as well as the degree of functionalization and the type of integrated DASAs. Integration of new monomers and comonomers will allow further improvement of the matrix properties in the future to provide optimized photoswitching properties by using ene-functionalized silicones. Importantly, the modular nature of the presented approach can be readily expanded with new FAs, or combinations thereof, and with additional aromatic amine ene-precursors to design absorbance and photoswitching profiles over the whole visible spectrum. That could be achieved with our new synthesis method using 1,1,1,3,3,3-hexafluoro-2-propanol as a promoter of the ring-opening reaction, what leads to both shortened reaction times in the DASA synthesis as well as the synthesis of previously unattainable DASAs.[13] In the future, the combination with fluorescent dyes in the matrix can allow both 2-photon-based writing and fluorescence-based reading. With the optimization of the 2PP process on high efficiency commercial microprinters, the presented methodology can enable direct laser writing of photochromic micro-objects for applications within complex microfabricated structures with high demands on their exact localization and shape.

Supporting Information

Supporting Information is available from the Wiley Online Library or from the author.

Acknowledgements

The Swiss National Science Foundation (SNSF) is acknowledged for the financial support through Grant Nos. 200021_172609 and PP00P2_172927. X.-H.Q. would like to acknowledge the financial support by a Marie-Curie postdoctoral fellowship (COFUND 267161), the SNSF Spark grant (No. 190345), and an ETH Zurich Career Seed grant (SEED21 18-2). X.W. would like to acknowledge the financial support by Shenzhen Institute of Artificial Intelligence and Robotics for Society (2020-ICP002). The authors thank Dr. Yinyin Bao (ETH Zurich) for critical reading of this manuscript.

Conflict of Interest

The authors declare no conflict of interest.

Data Availability Statement

Research data are not shared.

Keywords

3D-printing, donor–acceptor Stenhouse adducts, photochromism, thiol–ene reaction, two-photon polymerization

Received: April 4, 2021
Revised: April 26, 2021
Published online:

[1] J. C. Crano, R. J. Guglielmetti, *Organic Photochromic and Thermochromic Compounds*, 1st ed., Vol. *1*, Kluwer Academic Publishers, New York, USA **1999**.
[2] M. M. Russew, S. Hecht, *Adv. Mater.* **2010**, *22*, 3348.
[3] H. Tian, J. Zhang, in *Photochromic Materials: Preparation, Properties and Applications* (Eds: H. Tian, J. Zhang), Wiley-VCH, Weinheim, Germany **2016**, pp. 393–415.
[4] M. Irie, *Chem. Rev.* **2000**, *100*, 1685.
[5] A. C. Pauly, K. Schöller, L. Baumann, R. M. Rossi, K. Dustmann, U. Ziener, D. de Courten, M. Wolf, L. F. Boesel, L. J. Scherer, *Sci. Technol. Adv. Mater.* **2015**, *16*, 034604.
[6] K. Schöller, S. Küpfer, L. Baumann, P. M. Hoyer, D. de Courten, R. M. Rossi, A. Vetushka, M. Wolf, N. Bruns, L. J. Scherer, *Adv. Funct. Mater.* **2014**, *24*, 5194.
[7] L. Wang, Q. Li, *Chem. Soc. Rev.* **2018**, *47*, 1044.
[8] P. Xiao, J. Zhang, J. Zhao, M. H. Stenzel, *Prog. Polym. Sci.* **2017**, *74*, 1.
[9] D. Bleger, S. Hecht, *Angew. Chem., Int. Ed.* **2015**, *54*, 11338.
[10] S. Helmy, F. A. Leibfarth, S. Oh, J. E. Poelma, C. J. Hawker, J. Read de Alaniz, *J. Am. Chem. Soc.* **2014**, *136*, 8169.
[11] S. Helmy, S. Oh, F. A. Leibfarth, C. J. Hawker, J. Read de Alaniz, *J. Org. Chem.* **2014**, *79*, 11316.
[12] M. M. Lerch, W. Szymanski, B. L. Feringa, *Chem. Soc. Rev.* **2018**, *47*, 1910.
[13] M. Clerc, F. Stricker, S. Ulrich, M. Sroda, N. Bruns, L. F. Boesel, J. Read de Alaniz, *Angew. Chem., Int. Ed.* **2021**, *60*, 10219.
[14] J. R. Hemmer, S. O. Poelma, N. Treat, Z. A. Page, N. D. Dolinski, Y. J. Diaz, W. Tomlinson, K. D. Clark, J. P. Hooper, C. Hawker, J. Read de Alaniz, *J. Am. Chem. Soc.* **2016**, *138*, 13960.
[15] J. R. Hemmer, Z. A. Page, K. D. Clark, F. Stricker, N. D. Dolinski, C. J. Hawker, J. Read de Alaniz, *J. Am. Chem. Soc.* **2018**, *140*, 10425.

[16] Y. Chen, Z. Li, H. Wang, Y. Pei, Y. Shi, J. Wang, *Langmuir* **2018**, *34*, 2784.
[17] S. Jia, J. D. Du, A. Hawley, W.-K. Fong, B. Graham, B. J. Boyd, *Langmuir* **2017**, *33*, 2215.
[18] B. Mason, M. Whittaker, J. Hemmer, S. Arora, A. Harper, S. Alnemrat, A. McEachen, S. Helmy, J. Read de Alaniz, J. Hooper, *Appl. Phys. Lett.* **2016**, *108*, 041906.
[19] S. H. Mostafavi, W. Li, K. D. Clark, F. Stricker, J. Read de Alaniz, C. J. Bardeen, *Macromolecules* **2019**, *52*, 6311.
[20] O. Rifaie-Graham, S. Ulrich, N. Galensowske, S. Balog, M. Chami, D. Rentsch, J. Hemmer, J. Read de Alaniz, L. F. Boesel, N. Bruns, *J. Am. Chem. Soc.* **2018**, *140*, 8027.
[21] T. Senthilkumar, L. Zhou, Q. Gu, L. Liu, F. Lv, S. Wang, *Angew. Chem., Int. Ed.* **2018**, *57*, 13114.
[22] G. Sinawang, B. Wu, J. Wang, S. Li, Y. He, *Macromol. Chem. Phys.* **2016**, *217*, 2409.
[23] S. Ulrich, J. R. Hemmer, Z. A. Page, N. D. Dolinski, O. Rifaie-Graham, N. Bruns, C. J. Hawker, L. F. Boesel, J. Read de Alaniz, *ACS Macro Lett.* **2017**, *6*, 738.
[24] S. Ulrich, S. O. Moura, Y. Diaz, M. Clerc, A. G. Guex, J. Read de Alaniz, A. Martins, N. M. Neves, M. Rottmar, R. M. Rossi, G. Fortunato, L. F. Boesel, *Sens. Actuators, B* **2020**, *322*, 128570.
[25] B. Wu, T. Xue, W. Wang, S. Li, J. Shen, Y. He, *J. Mater. Chem. C* **2018**, *6*, 8538.
[26] J. E. Yap, N. Mallo, D. S. Thomas, J. E. Beves, M. H. Stenzel, *Polym. Chem.* **2019**, *10*, 6515.
[27] S. Chen, W. Li, W. Zhu, in *Photochromic Materials: Preparation, Properties and Applications* (Eds: H. Tian, J. Zhang), Wiley-VCH, Weinheim, Germany **2016**, pp. 71–108.
[28] M. M. Lerch, M. J. Hansen, W. A. Velema, W. Szymanski, B. L. Feringa, *Nat. Commun.* **2016**, *7*, 12054.
[29] S. Murphy, A. Atala, *Nat. Biotechnol.* **2014**, *32*, 773.
[30] X.-H. Qin, A. Ovsianikov, J. Stampfl, R. Liska, *BioNanomaterials* **2014**, *15*, 49.
[31] T. Wallin, J. Pikul, R. Shepherd, *Nat. Rev. Mater.* **2018**, *3*, 84.
[32] C. LaFratta, J. Fourkas, T. Baldacchini, R. Farrer, *Angew. Chem., Int. Ed.* **2007**, *46*, 6238.
[33] J. Torgersen, X.-H. Qin, Z. Li, A. Ovsianikov, R. Liska, J. Stampfl, *Adv. Funct. Mater.* **2013**, *23*, 4542.
[34] X.-H. Qin, X. Wang, M. Rottmar, B. J. Nelson, K. Maniura-Weber, *Adv. Mater.* **2018**, *30*, 1705564.
[35] C. E. Hoyle, A. B. Lowe, C. N. Bowman, *Chem. Soc. Rev.* **2010**, *39*, 1355.
[36] R. K. Iha, K. L. Wooley, A. M. Nystrom, D. J. Burke, M. J. Kade, C. J. Hawker, *Chem. Rev.* **2009**, *109*, 5620.
[37] a) J. Kumpfmueller, K. Stadlmann, Z. Li, V. Satzinger, J. Stampfl, R. Liska, *Des. Monomers Polym.* **2014**, *17*, 390; b) C. Barner-Kowollik, M. Bastmeyer, E. Blasco, G. Delaittre, P. Muller, B. Richter, M. Wegener, *Angew. Chem., Int. Ed. Engl.* **2017**, *56*, 15828.
[38] M. Morimoto, S. Kobatake, M. Irie, H. Bisoyi, Q. Li, S. Wang, H. Tian, in *Photochromic Materials: Preparation, Properties and Applications* (Eds: H. Tian, J. Zhang), Wiley-VCH, Weinheim, Germany **2016**, pp. 281–360.
[39] K. Shima, K. Mutoh, Y. Kobayashi, J. Abe, *J. Phys. Chem. A* **2015**, *119*, 1087.
[40] R. A. Evans, T. L. Hanley, M. A. Skidmore, T. P. Davis, G. K. Such, L. H. Yee, G. E. Ball, D. A. Lewis, *Nat. Mater.* **2005**, *4*, 249.
[41] a) S. C. Ligon, J. Kumpfmüller, N. Pucher, J. Stampfl, R. Liska, in *Multiphoton Lithography: Techniques, Materials, and Applications*, (Eds: J. Stampfl, R. Liska, A. Ovsianikov), Wiley-VCH, Weinheim, Germany **2016**, pp. 265–296; b) A. Ovsianikov, X. Shizhou, M. Farsari, M. Vamvakaki, C. Fotakis, B. N. Chichkov, *Opt. Express* **2009**, *17*, 2143.
[42] Y. Liu, W. Xiong, D. W. Li, Y. Lu, X. Huang, H. Liu, L. S. Fan, L. Jiang, J.-F. Silvain, Y. F. Lu, *Int. J. Extreme Manuf.* **2019**, *1*, 025001.